A Model for a Driven Frenkel-Kontorova Chain

W. Quapp[1] and J. M. Bofill[2]

[1] Mathematisches Institut, Universität Leipzig, PF 100920, D-04009 Leipzig, Germany
[2] Departament de Química Inorgànica i Orgànica, Secció de Química Orgànica, and Institut de Química Teòrica i Computacional, (IQTCUB), Universitat de Barcelona, Martí i Franquès 1, 08028 Barcelona, Spain

Abstract. We study a Frenkel-Kontorova model of a finite chain with free-end boundary conditions. The model has two competing potentials. Newton trajectories are an ideal tool to understand the circumstances under a driving of a Frenkel-Kontorova chain by external forces. To reach the insights we calculate some stationary structures for a chain with 23 particles. We search the lowest energy saddle points for a complete minimum energy path of the chain for a movement over the full period of the on-site potential, a sliding. If an additional tilting is set, then one is interested in barrier breakdown points on the potential energy surface for a critical tilting force named the static frictional force. In symmetric cases, such barrier breakdown points are often valley-ridge inflection points of the potential energy surface. We explain the theory and demonstrate it with an example. We propose a model for a DC drive, as well as an AC drive, of the chain using special directional vectors of the external force.

PACS. Frenkel-Kontorova model – DC- or AC-tilting – Newton trajectory – Barrier breakdown point – Valley-ridge inflection point

1 Introduction

In solid-state physics one often divides a set of particles in a one-dimensional subsystem of interacting elements, and in the remaining part as a substrate. The latter acts by a potential on the extracted subsystem. One example of such a model is the Frenkel-Kontorova (FK) model [1, 2]. It has the ability to account for many nonlinear problems. The one-dimensional subsystem is represented by a discrete chain of particles harmonically coupled with their nearest neighbors, while the action of the fixed substrate can be described by a sinusoidal form.

In many applications, one particularly interesting aspect of the FK model is its driven form. The concept has subsequently been involved in many applications of the model including alternating current (AC) driven models [2–6], or direct driven (DC) models [7–10]. Nowadays sliding friction forms a broad interdisciplinary research field that often involves the application of the FK model [8,10, 11] where the applications go up to earthquake research [12]. Zanca et al. recently remarked that 'friction is, among all basic physical phenomena, the one in most need of fundamental works' [13].

We here propose the usage of Newton trajectories (NTs) [14]. They describe the curve of the displaced stationary points under the increasing external force for every tilted potential energy surface (PES). To treat the PES of a physical problem is not new, however it is here the key

step for a deeper understanding. On the other hand, NTs are mathematical tools. They are curves on the given PES where at every curve point the gradient of the PES points into the same direction called the search direction [15]. With the help of NTs we find a low energy path for a full movement of the chain through the PES over a period of the site-up potential. The search direction of the NT is the tilting direction of a force to be applied to move the chain exactly along this pathway.

The paper has the following Sections: in Section 2 we report on the FK model which is then tilted in Sect. 3. A short review of the theory of NTs is added, and it is explained how NTs can be applied to the FK model. Section 5 describes an example of the $N{=}23$ FK chain. We get symmetric and asymmetric minimums and saddle points (SPs) of index 1 and 2. Here the particularity emerges that the global lowest transition state on a minimum energy path (MEP) for a movement of the chain by $\approx a_s$, the period of the sinusoidal potential, is a pair of two SPs of equal height in a row, with a valley-ridge inflection (VRI) manifold of points in between. Two such valleys emerge in the $N{=}23$-case, separated by an SP of index 2. The connection of the two corresponding SP_1 is a family of singular NTs. Using these mathematical findings, we propose a model for an overall tilting of the chain along its axis by a special DC force, as well as by an alternating AC force hopefully anticipating a corresponding experiment. The end is the Conclusion. Data are collected in a Supplemental Material (SM).

2 The FK model

2.1 Model formula

$\mathbf{x} = (x_1, .., ..., x_N)^T$ is a linear chain of N discrete particles. The positions x_i are on an axis. For all particles holds $x_i < x_{i+1}$. They are sorted in a fixed order. We treat a finite chain, thus N is less than infinity [14, 16–23]. The boundaries are free [24]

A spring force acts with a force constant k between the particles which would results in a constant natural distance a_o of the particles. Without the side force, the end points of the chain are such that the average distance is $a_o = (x_N - x_1)/(N-1)$. Different 'natural' distances are a possible generalization [25–28], as well as different spring constants, k_i [29], both of which we do not use here. A fixed on-site potential with a periodicity of a_s acts on the particles in concurrence with the springs. The sinusoidal potential mimics a rigid, not deformable substrate. The ratio a_o/a_s is named the misfit parameter. The PES for the variables x_i is the Frenkel-Kontorova model

$$V(\mathbf{x}) = v \sum_{i=1}^{N} [1 - cos(\frac{2\pi x_i}{a_s})] + \sum_{i=1}^{N-1} \frac{k}{2} [x_{i+1} - x_i - a_o]^2 . \quad (1)$$

We put the factor at the sinusoidal potential, $v=1$, throughout the paper. Then the spring constant, k, is also the ratio of the strength of the sinusoidal potential to that of the spring potential. Because $v > 0$, the sinusoidal potential will modulate the chain [30], and we will generally get another average spacing, $\tilde{a}_o$. All quantities referred to in this work are dimensionless.

2.2 Calculation of special structures of the FK chain

We use here the application of NTs as a method for the FK model [14]. For control reasons, we also use the optimization in Mathematica by "NMinimize". A further tool is steepest descent (SD). Barrier breakdown points (BBPs) are calculated by the Barnes method [31]. Valley-ridge inflection points (VRIs) are approximated by a scheme of Schmidt and Quapp [32, 33].

3 Tilting of the FK model

In atomic force microscopy, a cantilever pulls a molecule with a given force in a defined direction [23, 24]. Such a tilting can be applied also to an FK chain. Additionally to the two forces of the FK model, we use an external, linear force in the ansatz [1, 2, 14, 19, 26, 34–43]. We name the resulting PES an effective PES

$$V_F(\mathbf{x}) = V(\mathbf{x}) - F (l_1, .., l_N)^T \cdot \mathbf{x} . \quad (2)$$

The multiplication point between the normalized N-dimensional direction vector $\mathbf{l} = (l_1, .., l_n)^T$ and the N-variable $\mathbf{x}$ means the scalar product. The amount of the force is either given by the direct part, F_{dc} [7–10], or by an alternating part, $\pm F_{ac}$ [2–5]. The force tilts the former sinusoidal

potential with the incline F in direction $\mathbf{l}$. If $F=0$, then a minimum structure for the chain will exist. But if all $l_i > 0$, and if $F > 0$ is large enough, then a minimum does not exit [14, 19]. Interesting is the so-called pinning-depinning transition, as well as the backward process [20], compare also Section 4.3 below. The barrier for a depinning is reduced in the case of special misfit parameters between chain and substrate. It was named superlubricity [44–49].

4 Newton trajectories

4.1 The Definition

Tilting means that we now look for a stationary chain with $g_i(\mathbf{x}) = F l_i$, $i = 1, .., N$, F is the variable amount and the l_i are fixed. Such an ansatz is named Newton trajectory [50, 51] in the N-dimensional space of the particles, to a search direction $\mathbf{f} = F (l_1, .., l_N)^T$. The stationary points on the effective potential satisfy the vector equation

$$\nabla_{\mathbf{x}} V_F(\mathbf{x}) = \mathbf{g}(\mathbf{x}) - \mathbf{f} = \mathbf{0} . \quad (3)$$

One searches a point where the gradient of the original PES, $\mathbf{g}(\mathbf{x})$, has to be equal to the force, $\mathbf{f}$. The NT describes a curve of force-displaced stationary points (FDSPs) of the tilted PES under a different load, F [50–56]. Usually, the energy of a minimum can increase, but the energy of the next SP can be lower. This means that the barriers become lower.

The NT can be treated without the treatment of the physics of the external force in Eq.(2). One only needs an abstract search direction. Then any NT describes a connection between different stationary points of an index difference of one [57]. Following an NT is a method to search a next SP if a minimum is given, or vice versa.

We write Eq.(3) in projector form [50, 51]

$$\left(\mathbf{U} - \mathbf{l}\mathbf{l}^T\right) \mathbf{g}(\mathbf{x}) = \mathbf{0} . \quad (4)$$

$\mathbf{U}$ is the unit matrix and the $\mathbf{l}$-unit vector is the normalized direction of $\mathbf{f}$. The equation (4) then means that $\mathbf{g}$ and $\mathbf{l}$ are parallel. If we differentiate the projector Eq.(4) with respect to the parameter that characterizes the FDSPs curve, s in $\mathbf{x}(s)$, we obtain with the Hessian, $\mathbf{H}$ [51, 53]

$$\left(\mathbf{U} - \mathbf{l}\mathbf{l}^T\right) \mathbf{H}(\mathbf{x})\frac{d\mathbf{x}}{ds} = \mathbf{0} . \quad (5)$$

This is an expression of the tangent of the FDSPs curve. For the calculation, the continuous NT is approximated by L node points. The N particles of the chain form a point in the N-dimensional configuration space. A curve of such points is the NT. And it is numerically treated by its L nodes. We can easily calculate the Hessian of the FK model [14]. Then Eq.(5) is a way to generate the NT of a successive tilting. We use a predictor-corrector method for the calculations. For the predictor we use the tangent

of the NT with Eq.(5), or the growing string ansatz [58, 59]. The tangent of Eq.(5) also is employed for the corrector direction, back to the correct NT, with a Newton-Raphsen-like method [59].

Note, the amount of the tilting force, F, does not appear in Eq.(5). Thus the NT of the original PES for $F = 0$ does not change if we jump to a special effective surface, V_F, for a fixed l-direction and an $F > 0$.

4.2 Application of NTs to the FK model

We search for a minimum on the PES of the FK chain with the three steps:

(1) Build a natural chain with spacing a_o: Set, for example, $x_1=0$ for the initial particle, thus it is in the first well of the sinusoidal potential, and set $x_i = (i-1)\,a_o$ for $i = 2, .., N$.

(2) Use the natural chain in the PES of Eq.(1): it gives $V(\mathbf{x})$, and calculate the gradient $\mathbf{g}(\mathbf{x})$.

(3) Form the normalized direction $\mathbf{l}$ along the negative gradient: it is the search direction of an NT which goes through the surface point $V(\mathbf{x})$. Follow the NT downhill to the next stationary state which usually is a minimum.

(4) By turning the search direction starting at a minimum, we find SPs in the same way because NTs equivalently work downhill or uphill. This property is connected with the index theorem [57] which determines that regular NTs connect stationary points of an index difference of one.

4.3 Barrier breakdown points - BBPs

If one goes along the corresponding FDSPs curve with a given direction $\mathbf{l}$, then the magnitude of the gradient, equal to F, is zero at a stationary point of $V(\mathbf{x})$, and ends with zero at the final next stationary point. In between there has to be a maximum of $|\mathbf{g}|$. Here holds the condition [55, 60, 61].

$$Det(\mathbf{H}(\mathbf{x})) = 0 \qquad (6)$$

with the Hessian, $\mathbf{H}(\mathbf{x})$, of the original PES, $V(\mathbf{x})$. This is the point where the effective $V_F(\mathbf{x})$ along the FDSPs path has a shoulder [55,60,61]. The barrier of $V_F(\mathbf{x})$ decreases from the original PES barrier to zero. The point on the FDSPs curve is named the barrier breakdown point (BBP). Then the critical force, F_c, named the static frictional force [8], is so high that it causes the final depinning of the chain.

If we compare all NTs of a set which connect the same minimum and SP, then the NT which gives the lowest value of F_c is the *optimal NT*, and the point is named the *optimal BBP* [55,61]. The optimal BBP defines the lowest

maximal magnitude of the force. It satisfies the equation [55,61]

$$\mathbf{H}(\mathbf{x})\mathbf{g}(\mathbf{x}) = \mathbf{0} \quad \text{where} \quad \mathbf{g}(\mathbf{x}) \neq \mathbf{0} . \qquad (7)$$

At the optimal BBP the gradient is an eigenvector of the Hessian matrix to eigenvalue zero. The point belongs to a gradient extremal (GE) [62–68]. At the optimal BBP, the $Det(\mathbf{H}) = 0$-manifold, the GE and the optimal regular NT meet. An algorithm to locate optimal BBPs has recently been proposed [31]. The expression of the optimal BBP, Eq.(7), has a special form for the FK-model because of the tridiagonal shape of the Hessian, see Ref. [14].
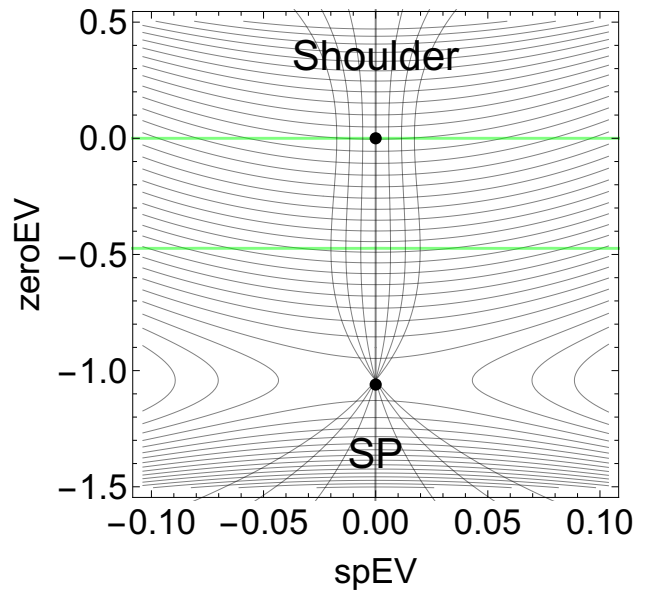
Fig. 1. 2D PES model around a ridge-shoulder (upper black bullet). A family of NTs is drawn starting at the SP to different directions. Only one NT crosses the shoulder, which behaves like an ordinary point of the PES. The green lines are BBPs of NTs.

4.4 Degenerated stationary points

On the PES of the FK model for $N=23$ particles many degenerated stationary points emerge. They are defined by the condition

$$|\mathbf{g}(\mathbf{x})| + |det\mathbf{H}(\mathbf{x})| = 0 . \qquad (8)$$

For NTs such points are quasi 'regular' points where the index theorem [57] does not apply. We demonstrate it by a simple 2D example in Fig. 1. (There are equidistant contours drawn by Mathematica, version 11.2, like all other figures of this paper). We study the behavior of NTs near a shoulder on a ridge where condition (8) is fulfilled.

The index theorem does not say what happens, because the shoulder is a stationary point of a 'half' index: the gradient is the zero vector, but also an eigenvalue of the Hessian is zero. The shoulder point behaves like an
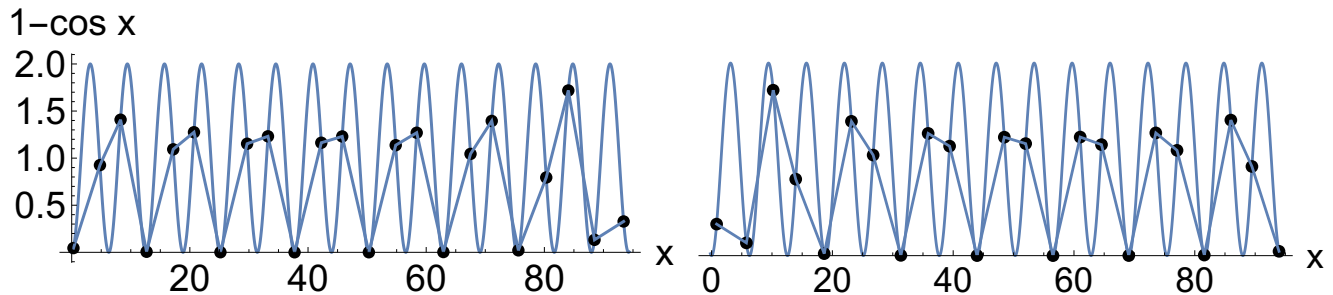
Fig. 3. Schematic picture of the structures of the 'left' asymmetric global minimum of the 23-particles chain, and its mirror image, the 'right' asymmetric minimum. The energy is 19.8242. Note that the particles are artificially set to the value of the (1-cos)-function. The real chain is linearly ordered on its axis. Only the distances between the x_i are changed by the on-site potential.
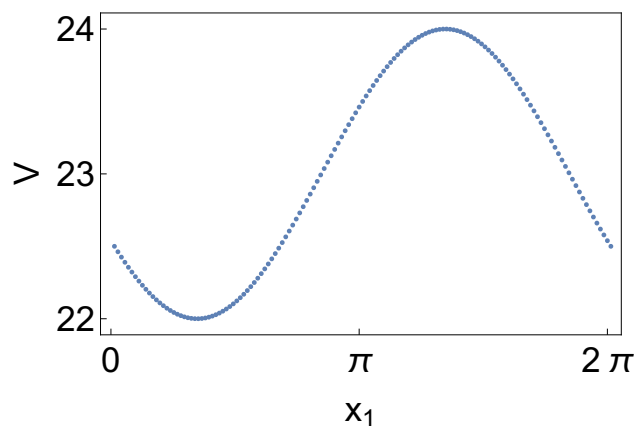
Fig. 2. Energy profile of the equidistant 23 particles (the natural chain) moved over the on-site potential as a fixed chain by a total distance of 2π. The horizontal axis depicts the location of x_1. The curve is a hint that for 'useful' connected structures, from one stationary point to the next at 2π distance, the energy should not exceed this 24 units mark.

ordinary point of the PES: exactly one NT crosses it. If the shoulder changes to an intermediate minimum, where the zero eigenvalue changes to a positive eigenvalue, then all NTs will cross it, like the SP.

5 Example of the FK Chain with 23 particles

Experiments with a chain of few tens of ions are done [24, 69]. The chain we will be looking at is the case N=23, with the parameters a_s=2π, a_0=$4\pi/3$, v=k=1 (thus the misfit parameter is 2/3).

For Fig. 2 we move the rigid natural chain with fixed equal distances, a_0, between all atoms, by 2π over the on-site potential and draw the energy profile. Because the on-site potential is fixed, we get different energies for the chain. We do not use an NT for the movement of the fixed chain, but the direction of the movement itself is the standard one, $(1,...,1)^T$. The minimum emerges at 22, the maximum at 24. The energy difference of the profile of Fig. 2 exhausts with 2 units the value of the $(1 - cos(x))$ function of the FK model [18]. Note that for the natural

chain the part of the spring energy is zero. At the mean energy, 23, the 23 cosine terms of $V(\mathbf{x})$ also add to zero; it only remains $V = \sum_1^{23} 1$=23. The minimum of the curve at $x_1 = \pi/3$ is a hint for a search of a better real minimum of the structure, in another position, and of course, with another $\tilde{a}_0$, in comparison to the natural chain, see the next subsection. Any useful SP of the structure should not overcome the 24 units obtained here because this natural structure would be such an SP, in a first approximation. However, the movement of the chain for Fig. 2 is an abstract one.

5.1 Global minimums

We have reported [14] two low minimums, as well as a low lying SP of index one in between. The minimums are asymmetric, but the SP is symmetric. The two mirror image minimums are shown in Fig. 3. Their energies are $V(min)$=19.8242. The SP has an energy of 19.9644. For the minimum is $\tilde{a}_0$=4.12, quite near to the natural a_0=4.19. The data of the minimum structures are given in the SM, Sect.1.1. and 1.2. The 23 particles of the chain are distributed to 16 wells of the sinusoidal potential. The occupation numbers 1 and 2 alternate here.

If we imagine a movement of the chain from the 'left' minimum to the 'right' minimum, one has to move in a first step up to the SP the atoms x_{15}, x_{18}, x_{21} into a new well but the x_{12} to the top between two wells. On the other side downhill to the 'right' minimum, the x_{12} is moved into its new well, and the atoms x_3, x_6, x_9 move into a new well. Note the triple numbering of the moving atoms, and note that the SP has only its central atom x_{12} at a top of the on-site potential. So it appears like a stable structure.

At the outer sides of the two minimum wells we tried to continue an NT to the standard direction $(1,...,1)^T$. It is possible to calculate a continuation, but the NT does not meet a stationary point up to an energy of over 22. After passing some higher turning points (TPs), the NT later finds the 'global' SP at an energy 21.2106, see below. This means that useful NTs of the chain, along a lower energy, go on by other, sectional directions. Below we add some results.
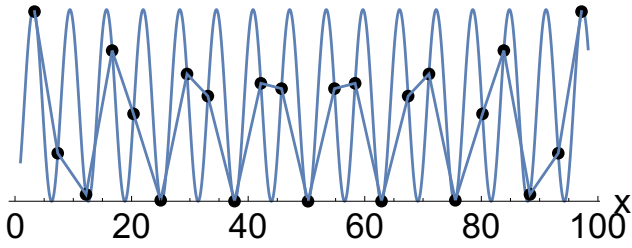
Fig. 4. An SP of index 2 of the 23-particle chain depicted by SP_2 in the simplified Fig. 5. The energy is 22.099. It is symmetric.

5.2 Global low energy pathways

In an NT calculation we found an SP of index 2 at an energy 22.099, see Figs. 4 and 5 and data in the SM, Sect. 2.1. It is a central point for a system of low energy valleys of the FK model (1) with $N=23$ particles and the given parameters. The reason is that it is connected by a steepest descent with a minimum of a chain in normal position (x_1 is in the zero well of the site potential like in Fig. 3), and with a complementary minimum on the other side of the PES mountains moved by $a_s = 2\pi$ over the sinusoidal potential. This is the aim: we search for a recurrence of the initial state of the chain moved over the site-up potential.
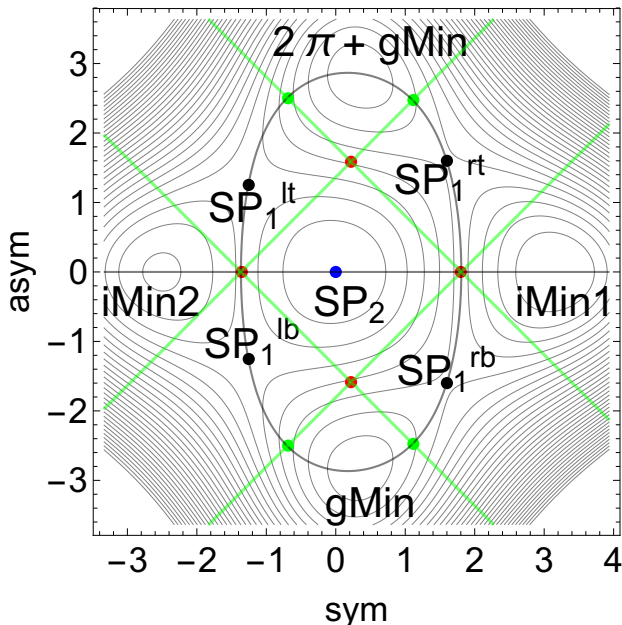
Fig. 5. A region of the PES is approximated around the global SP_2 at $(0,0)$. The axes are the two negative eigenvectors of the full Hessian at the SP_2. They are symmetric or asymmetric directions. The thick curve is a singular NT to direction 'sym'. The 4 red points are VRI points. The green bullets are BBPs of the singular NT, and the net of green lines indicates Det(H)=0. The description of the SPs of index 1 goes with 'l' for left, 'r' for right, 'b' for bottom, and 't' for top, in this Figure. gMin depicts the two (global) minimums of the (full) PES. In this 2D simplification of the PES the iMin1 is still deeper.

The SP_2 has two equal negative eigenvalues of -0.3813. To give an image of the region around this top we draw a 2D sectional picture of the PES of the FK model (1) for $N=23$. We used the two negative eigenvectors of the SP_2 for the plane of the picture, the data are in the SM, Sect. 2.1. The points of the plane are obtained by the linear ansatz $\mathbf{x}(s,a) = SP_2 + s\,EV_1 + a\,EV_2$ and are included in the energy function, $V(\mathbf{x})$. The result is Fig. 5. It is a representation of the simplified energy function $V_{SP2}(\mathbf{x}(s,a))$ by level lines. Note that it is a 2D section. The point $(0,0)$ is exactly the SP_2, however, stationary points lying displaced may not be correctly represented.

Since 30 years, SPs of index 2 are discussed in theoretical chemistry [70–77]. Here emerges a possible
Characterization of an SP_2:

– From a usual SP of index 1 one can expect to go down by the SD into two different minimum valleys using for the first step the eigenvector to the negative eigenvalue.

– From an SP of index two one can hope that it is possible to go down by the SD into up to four different minimums using for the first step the two eigenvectors to negative eigenvalues. (But many other cases are possible; one is studied in Refs. [78,79]).

We have four SPs of index one on a circle around the SP_2. On the full 23-dimensional PES of the chain we localized the corresponding stationary points. The left two are on the level 21.1699, the right two at the slightly higher energy 21.2106 (in contrast to the relation in Fig. 5). The data are in the SM in Sect. 2.2. An equipotential line connects the two left SP_1^l, as well as another equipotential line connects the two right SP_1^r. The corresponding pieces are part of an NT to direction 'sym', here in this simplified 2D picture. It means that all gradients of the 2D sectional PES on this curve point into 'sym'-direction. Note that the NT can pass a point where its tangent is orthogonal to the gradient: at the symmetric valley-ridge inflection (VRI) points.

From 'gMin' at the bottom of Fig. 5 to '2π+gMin' at the top, we find two valleys through the PES, one may be the minimum energy path (MEP) over the two lower SPs of index one, but the other is a low energy path (LEP) quite parallel to the former. Which valley we choose for a movement of the chain by a tilting force depends on the direction of the describing NT of the corresponding valley, see the description below.

The singular NT divides the two different valleys. It has a branch which forms the line $asym=0$ in Fig. 5. The two red points on the line are the bifurcation points of the NT which are VRI points of the surface between the two intermediate minimums, iMin, and the SP_2. Thus the NT is a singular NT [51]. (Two other asymmetric VRI points are also included in the Figure, near the sym=0 line at the green crosses. The corresponding singular NTs through the asymmetric VRI points are given in Figs. 6 and 7.) The symmetric VRI points on the line $asym=0$ are also BBPs because they are intersected by two green lines. But we cannot classify these BBPs to be 'optimal'
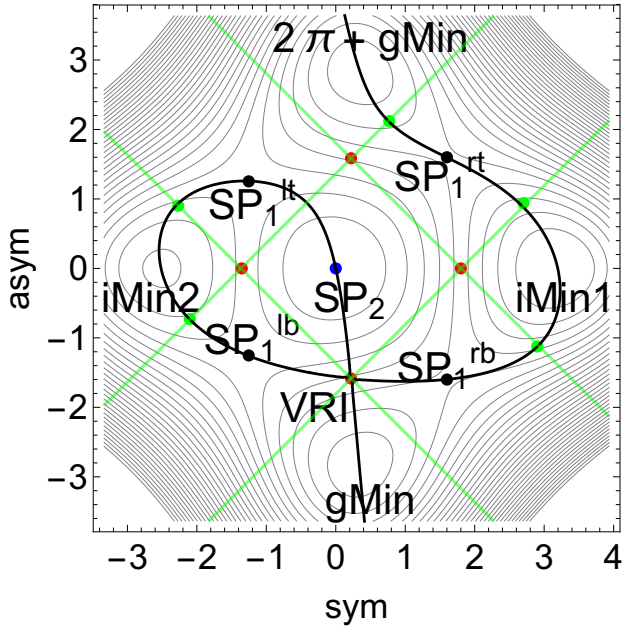
Fig. 6. The singular NT through the 'lower' asymmetric VRI point in the 2D simplified PES of Fig.5.
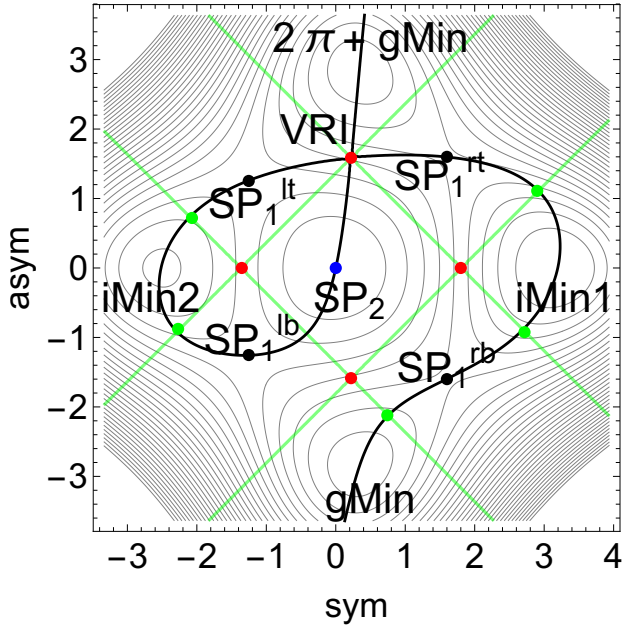
Fig. 7. The singular NT through the 'upper' asymmetric VRI point in the 2D simplified PES of Fig.5.

because the NT is singular. Other NTs for a comparison do not connect the two SP_1^l, or the two SP_1^r, because of the index theorem [57]. On the line $asym=0$, of course, it holds at the BBPs that $|\mathbf{g}|$ is a maximum. Such a maximum fits well the NT theory at VRIs [55].

Figure 8 represents a regular NT through the two 'right' SP_1. The structure of the SP_1^{lb} is shown in Fig. 9, where the structure of the SP_1^{rb} is shown in Fig. 10. The SPs at the top of the corresponding Fig. 5 are mirror structures
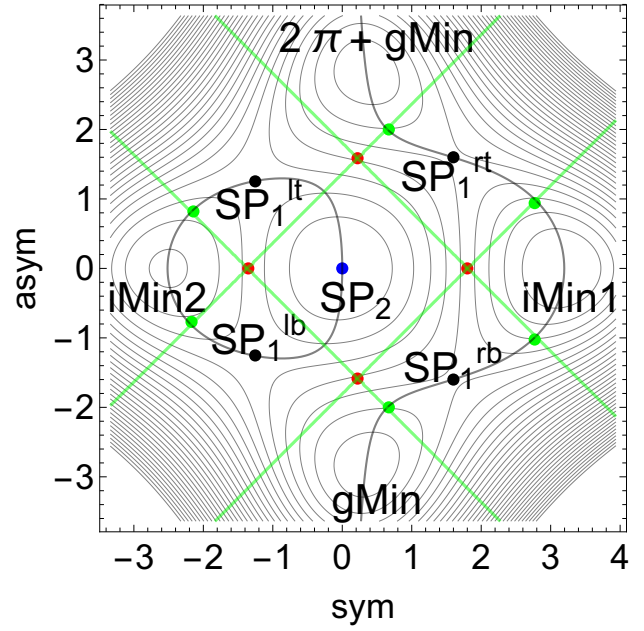
Fig. 8. The regular NT to direction 'asym' connects the two global minimums over the two 'right' SP_1 and the 'right' intermediate minimum, on the simplified 2D plane. Thus it could be one of the NTs of interest for a global low energy path of the chain.
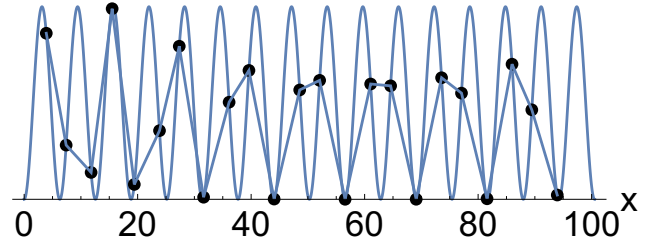
Fig. 9. The SP_1^{lb} of the 23-particle chain, compare Fig. 5. The energy is 21.1699. It is asymmetric. Its mirror structure is SP_1^{lt}.
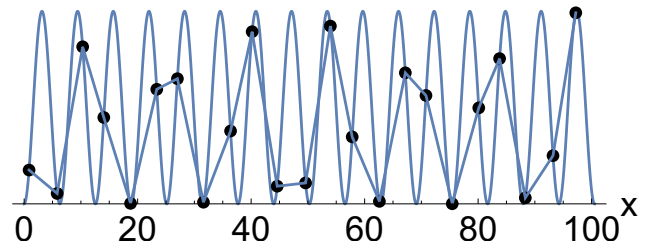
Fig. 10. The SP_1^{rb} of the 23-particle chain, compare Fig. 5. The energy is 21.2106. It is asymmetric. Its mirror structure is SP_1^{rt}.

of the SPs below. The data are in the SM, Sect.2.2. The NT of Fig. 8 may be one of the interesting NTs which describes a low energy path of the chain over a distance of 2π, the periodicity of the site potential. Below we will examine its use in the full 23D coordinate space.

Note that NTs are sometimes good models for reaction pathways over a PES. Here they serve for paths which de-

scribe the FDSPs curve. They connect different stationary points in an understandable and continuous way, and they can be used for a tilting of the chain into the corresponding direction.

Another method for the study of the PES is the steepest descent (SD) from the upper stationary points. Thus, the global connection of the region around SP_2 is easy to explore by the SD for the full 23-chain. We can start the SD curves at the SP_2 in the direction of its negative eigenvectors, or at the corresponding SP_1 in a diagonal direction. We have 4 valleys going downhill; two meet at the bottom and two at the top of Fig. 5, which we always use for the illustration but leaving out the other hidden 21 dimensions of the full chain. Two other valleys meet at the intermediate iMin1, and two at the intermediate iMin2. Thus SP_1^{lb} connects the global 'right' minimum with iMin2, SP_1^{lt} connects the global 'left' minimum+2π with iMin2, SP_1^{rb} connects the global 'right' minimum with iMin1, and SP_1^{rt} connects the global 'left' minimum+2π with iMin1. This means equivalently that the vertical direction of the NT leads to the global 'right' minimum below, and to the global 'left' minimum $+2\pi$ at the top. Thus, a vertical pathway like one of the corresponding branches of the shown NT of Fig.8 will form a global low energy path of the chain. The first peculiarity is that here are two competing ways, one on the left hand side, and one on the right hand side. The second peculiarity is that there are two SPs of index one in a row. A LEP on the tilted PES of the chain would have to pass both SPs on one side, one after the other.

For the full 23-chain, location and energy change for the numerical relations between the diverse stationary points, however, the 'topological' relations continue to stay like in Fig. 5.
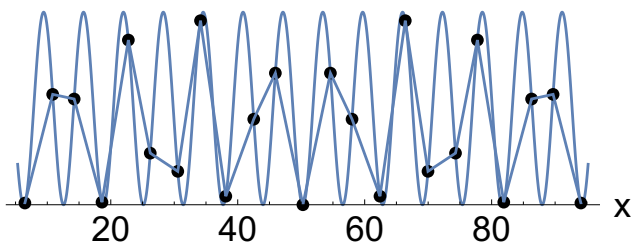
Fig. 11. 'Left' intermediate minimum 2 of the chain. The energy is 20.6556. It is symmetric. It is a compressed structure.

The horizontal direction along the $asym = 0$ line leads downhill from SP_2 to two intermediate minimums. This is also the result of a steepest descent in the $\pm$-symmetric direction from the SP_2. The structure of the minimums is shown in Figs. 11 and 12; and the data are in the SM, in Sect. 3. The intermediate minimum, iMin2, is symmetric. It is a compressed structure, $\tilde{a}_0=3.98$. The ends of its structure are pushed into the center by $\approx 2\pi$. The intermediate minimum, iMin1, is also symmetric, but it is a stretched structure, $\tilde{a}_0=4.48$ (remember $a_0=4.19$). An
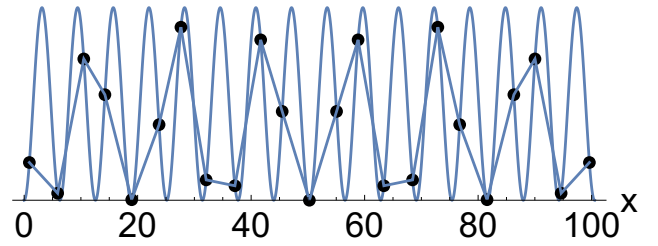
Fig. 12. 'Right' intermediate minimum 1 of the chain. The energy is 20.437 units, and it is also located on the symmetry hyperplane of the PES. It is a stretched structure.

imagination of a vibration between the two intermediates "flowing" around the SP_2, more or less in the symmetric hyperspace of the chain, would be a 'breathing' of the chain, but not a translation of the chain by 2π. On the other hand, the intermediate minimums are connected over the SPs of index 1 to the corresponding global minimums. Thus one can imagine an LEP on the PES of the chain from a global minimum over one of the SP_1 to the corresponding intermediate, and then it finds the exit over the mirror SP to the next global minimum: it could be the scenario of a global movement of the chain by $a_s = 2\pi$.
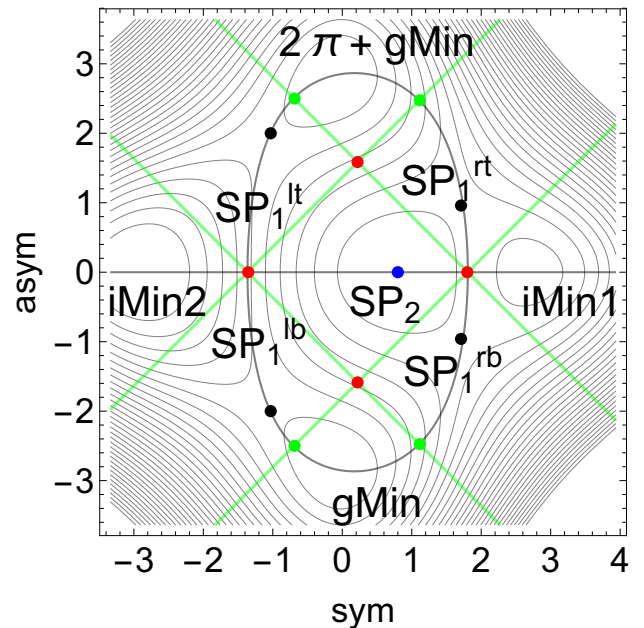
Fig. 13. Tilting the PES to the left hand side by a force into 'sym' direction. All stationary points move on the NT.

The question emerges: is the knowledge of the circle of SPs of index 1 around the SP_2 usable for a moving direction of the chain? Mathematically it is a singular NT through a VRI point at an end of the bowl of one of the intermediate minimums. Below we will examine its use in the full 23D coordinate space. First we treat the simplified 2D-case of Fig. 5 for a demonstration of what should happen. We have to take into account that the NT in Fig. 5 which connects all the interesting points is a singular NT.
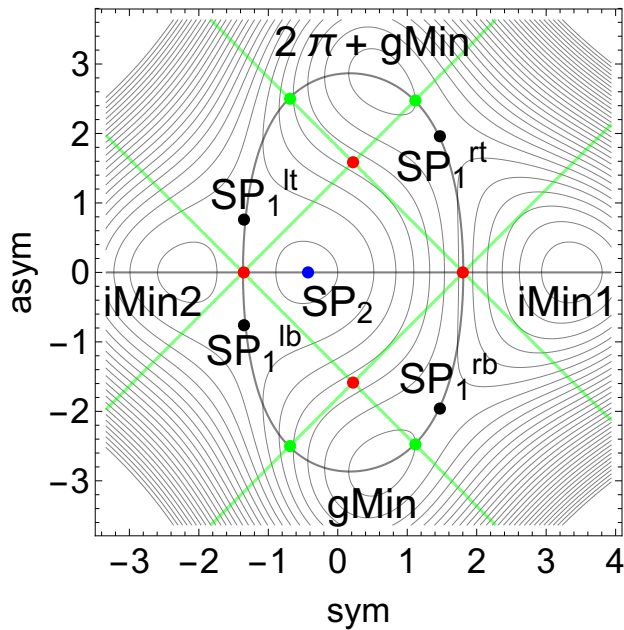
Fig. 14. Tilting the PES to the right hand side by a force into minus 'sym' direction.
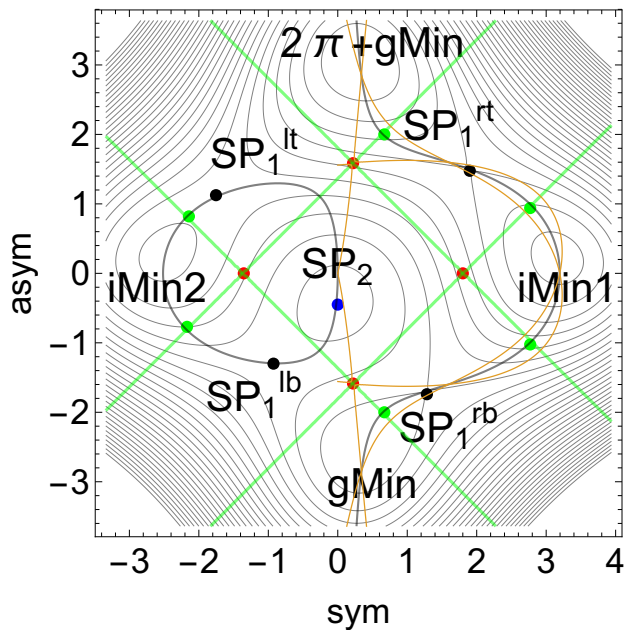
Fig. 15. Tilting the PES to the top of the region by a force into 'asym' direction with F=0.275. The light brown curves are two singular NTs through the asymmetric VRIs (see Figs. 6 and 7) which are the borders of the channel for a useful regular NT [56].

Now we tilt the chain along the direction of the singular NT, by an external force $\pm F\, EV_{sym}^T \cdot \mathbf{x}$.

It reduces to an effective surface

$$V(s,a)_{eff} = V_{SP2}(\mathbf{x}(s,a)) \pm F\, s \ . \qquad (9)$$

On the line $asym = 0$ the tilting moves together, or moves apart, the symmetric stationary points: the SP_2 and alternatively the two symmetric intermediate minimums.

For a moderate $F > 0$, say 0.2, it moves together the SP_2 and the right symmetric minimum. This means that the iMin1 is increased in energy, see Fig. 13. Under this action, the two right SP_1^r also move up in energy, so that the two left SP_1^l become much lower, and the MEP clearly goes over the left iMin2. But the level lines between the left, as well as the right SP_1 survive because the SPs move together on the singular NT which also survives.

For a moderate $F < 0$ the tilting moves together the SP_2 and the left symmetric minimum, vice versa to the former case, see Fig. 14. At least, for a critical F_c, the 2D-summit of SP_2 and the corresponding former intermediate minimum coalesce, as well as the two SP_1, and only one path along the level line along the singular NT remains. A corresponding strong tilting makes the corresponding symmetric, former intermediate minimum to the global minimum, at least on the simple 2D section of Fig. 5.

On the other hand, a tilting along the asymmetric eigenvector, in vertical direction in Fig. 5, leads at least to a dramatic disappearance of one global and the left intermediate minimum, and of the SP_2, and of three SP_1, compare Fig. 15. For F=0.275 the global minimum at the bottom (with x_1 near 0 on the axis) and the right intermediate minimum 1 survive. For F=-0.275 the global minimum at the top (with x_1 near 2π on the axis) and again the right intermediate minimum 1 survive.
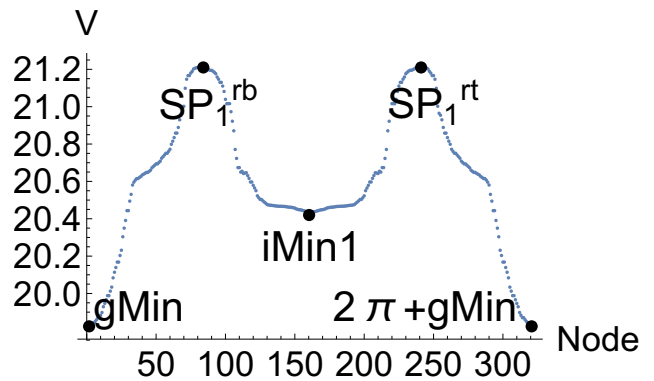
Fig. 16. Energy profile over a quasi 'minimal' pathway on the PES crossing the two SP_1^r at 21.2106. Shown is a combination of 4 NTs. The two left NTs are calculated to the SP-eigenvector at the bottom-SP_1^{rb}, where the two right NTs are calculated to the SP-eigenvector at the top-SP_1^{rt} which is the mirror vector to the former direction. Start is in all cases the corresponding SP, and the four pieces are combined. At the iMin1 two NTs cross which belong to different directions. All stationary points are depicted by black bullets.

Now we leave the tool of the 2D approximation of Fig. 5, even though we already had associated corresponding patterns of the approximation with real structures of

the chain. For the 23-chain, we first show a connection between the two right SP_1^r by two different NTs in Fig. 16. The search directions are the two SP directions. The combined curve opens a connection between the two global minimums, one at the initial location, but the second at a 2π moved structure. An external stimulation in the corresponding directions would need an AC-like force for a first step to move the chain into the iMin1, and a second step to move it to the 'upper' global minimum. However, it seems quite complicated to generate such forces because not only the $\pm$ changes are needed but also a change of the direction to its mirror direction in the 23D space.

In Fig. 17 is shown the same calculation for the SPs of index one on the left hand side of the SP_2.
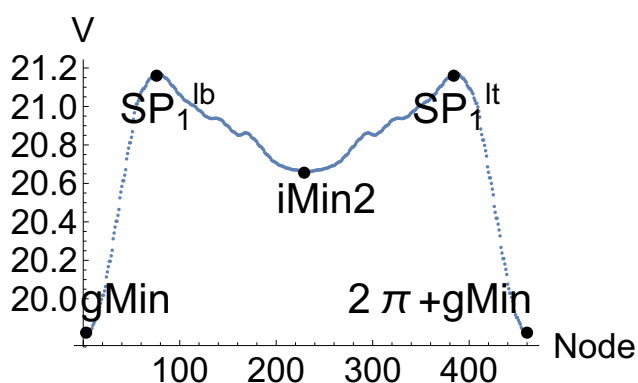
Fig. 17. Energy profile over an MEP on the PES crossing the two SP_1^l at 21.1699. The two left NTs are calculated to the SP-eigenvector at the bottom-SP_1^{lb}, where the two right NTs are calculated to the SP-eigenvector at the top-SP_1^{lt}. Start is in all cases the corresponding SP, and the four pieces are combined. At the iMin2 two NTs again cross which belong to different directions. All stationary points are depicted by black bullets; further small peaks of the inner NTs are turning points (TPs).

5.3 Symmetric VRI points between iMin$_1$ and SP$_2$

To guess the search direction for singular NTs is possible [32,33]. In full 23 dimensions, we first test the NT to the 'sym' direction of the SP_2: does it fulfill the task as it does in the simplified 2D case to be a singular NT? The proof is doing an NT calculation to the negative symmetric eigenvector direction of the SP_2. The (more or less) positive result is given in Fig. 18. It is an automatic detection of a VRI point to the sym-direction of the SP_2. This takes place by the NT to the given direction starting at the SP_1^{rb}. The energy profile over the NT crosses the symmetry subspace of the chain at the corresponding VRI point at 21.46, see Fig. 18. However note that the level of this VRI point is quite higher than the level of the SP_1^r. So one can guess that the sym-direction of the SP_2 is not an optimal direction for an external stimulation of the chain.
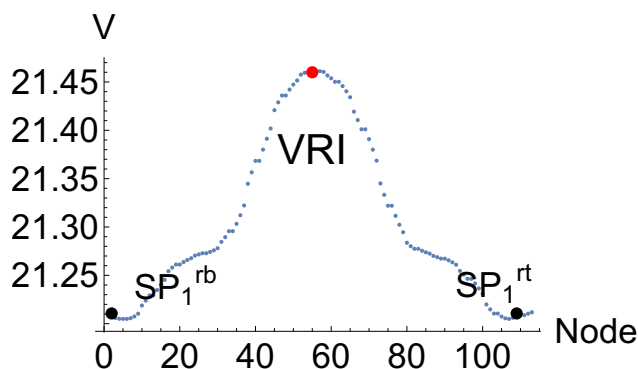
Fig. 18. Energy profile over an NT to the symmetric EV-direction of the SP_2. Start is the SP_1^{rb} where the NT follows the direction up to the VRI point at 21.46. The NT follows the mirror branch after the VRI to the SP_1^{rt}.

The search of further symmetric VRIs is done by the variational program of Schmidt and Quapp [32,33]. The aim is to find a 'better' singular NT which connects the two right central SP_1^r over this VRI point. The NT will be a tool to push and pull the FK chain globally over the PES by 2π. Three further VRIs are detected by test calculations. We assume that between them a manifold of VRI points exists [57,80–83].

Remark: The chemical community ignores the fact, up to date, that usually not only a single VRI point exists, but the VRIs are connected in a larger VRI-manifold. It is like in the case of conical intersections. Here we have the same problem of the 'unimaginability' of higher dimensional connected points of such a character, see Refs. [84, 85] and further references therein.

The data of the VRI points are given in the SM, Subsect. 3.3. The VRI1 is at energy 20.6710 with $|Ag|$=1.459E-002. (A is the adjoint matrix to the Hessian, H. $|Ag| = 0$ is the VRI criterion.) The NT to the corresponding direction of the gradient here, by the growing string method [58,59,78] is shown in Fig. 19 together with other NTs. The curve in the symmetric subspace of iMin$_1$ and SP_2 is well calculated with convergent corrector steps. We use here the growing string method to really enforce the NT to finish at the SP_2. It thus has to cross the VRI point on its way; but it does not break out to a side branch of the singular NT to one of the two SP_1^r. (In the next Subsection we use the other kind of calculations following the tangent of the NTs.)

The VRI2 is at energy 20.92 with $|Ag|$=3.843E-003. The next corresponding NT is shown again in Fig. 19. The VRI3 is at energy 21.0913 with $|Ag|$= 1.507E-003. The level of this VRI point is nearest to the corresponding SP_1^r-level. The structure of the VRI3 point is shown in Fig. 20. The NT is shown in Fig. 19. The NTs to the 3 lower VRIs all show a turning point. Nevertheless, they are fully in the symmetric subspace of the 23-chain. Note additionally that the curves are depicted over their nodes of the NT calculation. The distances in the coordinate

space, from node to node, may be not equidistant because of the predictor-corrector scheme of the calculation.
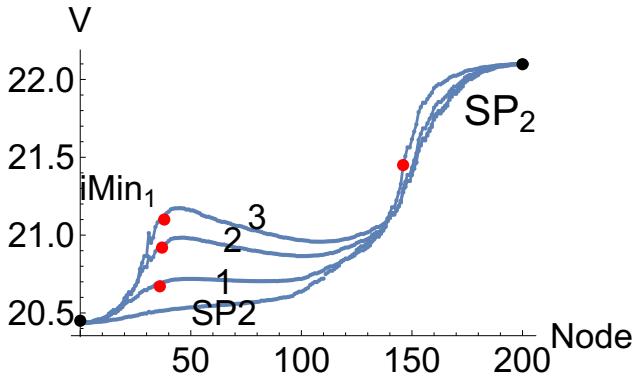
Fig. 19. Comparison of the energy profiles over NTs in the symmetric subspace to the directions of the 3 calculated VRIs (to numbers 1-3) between $iMin_1$ and SP_2, and the NT to the direction of the lowest symmetric EV of the SP_2. For the other branches of one of the NTs, compare Fig. 18. The VRI points are represented by red bullets.
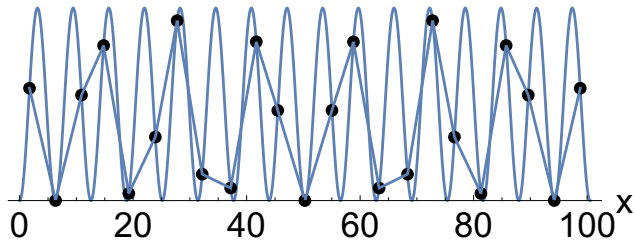
Fig. 20. The structure of the symmetric VRI3 point.

5.4 Branches of the singular NT between the two SP_1^r and the $iMin_1$

The found 3 VRI points deliver the directions for 3 singular NTs which connect the two SP_1^r, and which also have a branch to the intermediate iMin1. They are calculated with an NT following program using the tangent of the NTs with Eq.(5) for a predictor step. The results are shown in Figs. 21 to 23. Now the calculation of the corresponding NTs can jump to a side branch of the singular NT at the VRI point, in Fig. 21 and in Fig. 23 as well. Interestingly, in Fig. 22 the NT follows the tangent and jumps over the VRI point to the other side branch.

5.5 Singular NTs between the two SP_1^l and the $iMin_2$

We will again get an automatic detection of the VRI to the sym-direction of the SP_2 starting now at the left SP_1^{lb}. The energy profile over the NT crosses the symmetry subspace
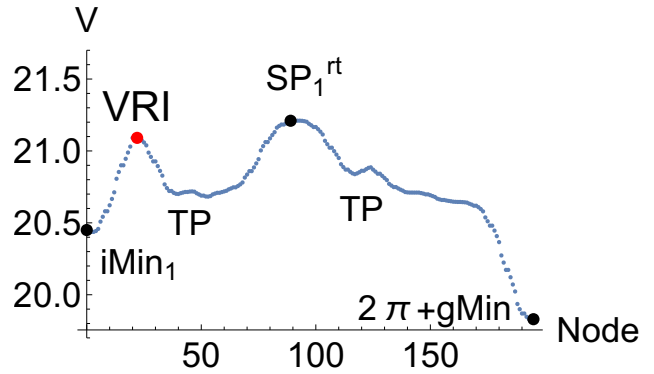
Fig. 21. Energy profile over an NT to direction of the symmetric VRI3 point. Start is the iMin1 where the NT follows the direction to SP_2 uphill up to the VRI point at 21.091. There it jumps to one of the crosswise branches from the VRI point to the SP_1^{rt} of index 1. The NT crosses the SP and goes further downhill to the global minimum moved by 2π. Further seemingly peaks are TPs.
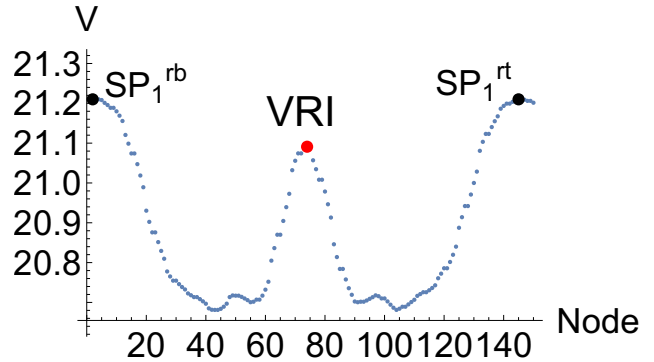
Fig. 22. Energy profile over an NT to direction of the symmetric VRI3 point. Start is the SP_1^{rb} where the NT follows the direction to the VRI point at 21.091. It follows the mirror branch after the VRI to the SP_1^{rt}. The branch between the VRI point and the SP_1^{rt} is also a part of Fig. 21.

of the chain at the corresponding VRI point at 21.687, see Fig.24. Note that the level of this VRI point is quite higher than the level of the SP_1^l. So one can guess that the sym-direction of the SP_2 again is not an optimal direction for a stimulation.

6 Calculations on the tilted PES

6.1 Symmetric force AC driving to new stationary states

We apply Eq.(2) with the direction vector being the gradient at a selected VRI point of the symmetric subspace of the chain, $(g_1, ..., g_N)^T$. The vector is also symmetric. For Fig. 25 we use the gradient vector of the VRI3 as an example. To make the profiles for different amounts, F, comparable, we represent relative energies. The global minimum (moved by 2π) at the end of the NTs (on the right hand
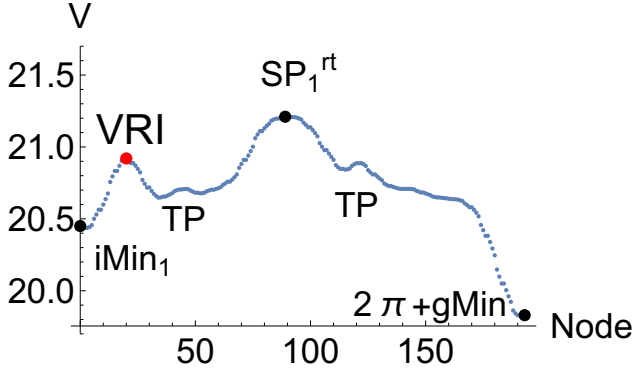
Fig. 23. Similar energy profile over an NT to direction of the symmetric VRI2 point, like in Fig.21. Start is again the iMin1 where the NT follows the direction to SP_2 uphill up to the VRI point at 20.92.
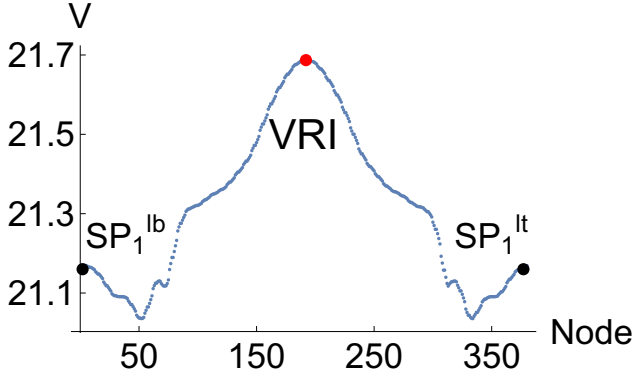
Fig. 24. Energy profile over an NT to symmetric EV direction of the SP_2. Start is the SP_1^{lb} where the NT follows the direction to the VRI point at 21.57. It follows the mirror branch after the VRI to the SP_1^{lt}.

side) is always put to zero. Near the factor F=-0.15 the $iMin1$ and the former global minimum change the order: the intermediate minimum becomes the global one. A similar scheme of NTs exists for the other side of the $iMin1$ valley, for the connection from the global minimum (beginning with x_1 in the zero-bowl of the site-potential) over SP_1^{rb} to the $iMin1$. On the other side of the SP_2, the $iMin2$ is increased in energy, for the used tilting, compare Fig. 14.

With usual thermodynamics, one can assume that under such a force the chain jumps from a global minimum to the $iMin1$, if the system temperature is higher than the remaining SP. If the force is stopped, the chain can relax, and by the symmetry, it will jump back with a probability 1/2 to the global minimum, or to the global minimum moved by 2π. Thus, with probability 1/2 we would get a global movement of the chain for such an AC driven system. Interestingly, the driving direction along a symmetric VRI-gradient will be orthogonal to the global moving direction of such a process.
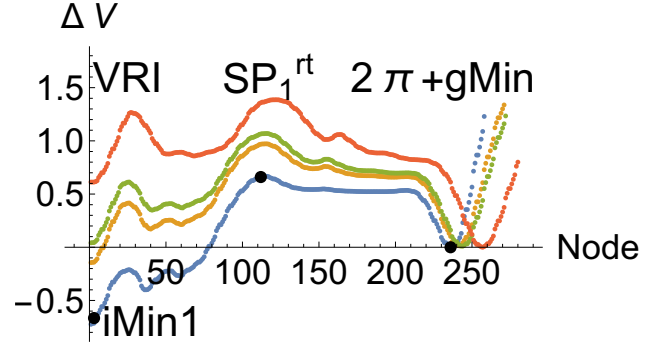
Fig. 25. Tilting of the chain. Relative energy profiles over NTs to the symmetric gradient direction of the VRI3. One can imagine the profiles as MEPs on the effective PESs (where the peak at the VRI point can be omitted). Start is the $iMin1$ on the left hand side. The NT follows the valley to the VRI point, then turns to the SP_1^{rt} and goes downhill to the global minimum moved by 2π. All curves are fixed at zero at the former global minimum, for better comparison. From top to bottom we used the factors F=0, -0.15, -0.2, and -0.35. The red curve for F=0 corresponds to the not tilted NT in Figs. 21 and 22.

6.2 Asymmetric force DC driving to new stationary states

We use the first asymmetric eigenvector to the negative eigenvalue of the central SP_2. The energy profile of a continuous NT starting at the global minimum to this direction is shown in Fig. 26.
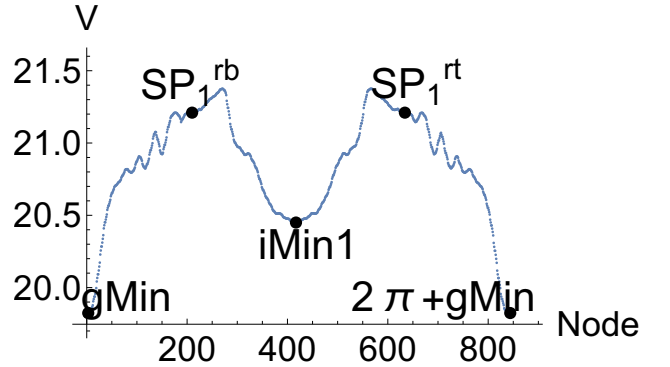
Fig. 26. Energy profile over the NT to the asymmetric negative eigenvector at the SP_2. Start is the global minimum on the left hand side. The NT follows the valley uphill to the SP_1^{rb}, then turns to the intermediate minimum, iMin1, goes further uphill to SP_1^{rt}, and after crossing it, the NT goes downhill to the global minimum moved by 2π. All stationary points are marked by a black bullet; further small peaks are turning points of the NT at the slope of the PES.

We again apply Eq.(2) with the direction vector being the negative asymmetric eigenvector of SP_2. We use F=0, -0.05, and -0.1 in Fig. 27. To make the profiles for the different amounts of F comparable, we show relative energies. The global minimum (moved by 2π) at the end

of the NTs (on the right hand side) is always put to zero. With usual thermodynamics, one can assume that under such a force the chain crosses from the global minimum to the iMin1, if the system temperature is higher than the remaining SP. The way to the other global minimum moved by 2π is still easier then. The blue curve may describe the stationary points of such a DC driven system.
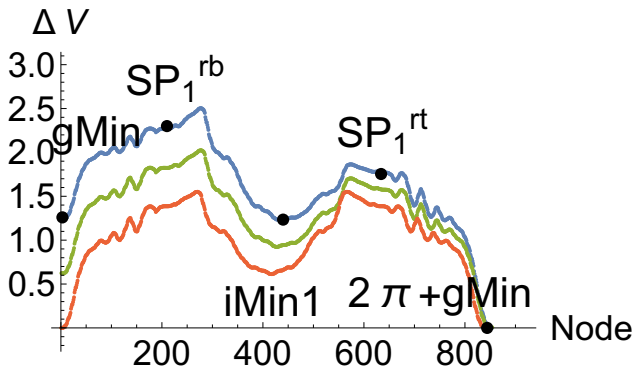
Fig. 27. Tilting of the chain. Relative energy profiles over NTs to the asymmetric negative eigenvector of SP_2. Start is the global minimum on the left hand side. The NT connects the SP_1^{rb}, the iMin1, the SP_1^{rt} and the global minimum moved by 2π. All curves are fixed at zero at the former final global minimum, for better comparison. From top to down we used the factors $F=0.1$, 0.05, and 0.0. The red curve for $F=0$ corresponds to Fig. 26. Compare the result with the schematic representation in Fig. 15 as well.

At the end of this subsection we remark that finding such an asymmetric driving direction, in a general high-dimensional PES, may be difficult. One has to detect the narrow pass, here for one dimension of the 23 dimensions of the chain, which meets the region of the central SP_2. A 3D schematic picture of the former Fig. 5 may illustrate this, see Fig. 28.

6.3 Push and pull force DC driving to new stationary states

The asymmetric direction for a driving force in Subsection 6.2 may be quite complicated to realize for an experiment. But a main property of the direction is that the main components of the force are concentrated at the periphery. This is why we tried a simpler direction, $(1,0,...,0,1)^T$, like it was used also in the case $N=5$ in Ref. [14]. The NT to the direction is successful for a connection of the global minimum over the SP_1^{lb} to iMin2 and over the SP_1^{lt} down to the 2π moved global minimum. Note: it is the other way around the SP_2, over the iMin2, in contrast to the direction of subsection 6.2. The profile over the NT is shown in Fig. 29

The used push and pull force is overwhelmingly simple. A scheme of the tilting for the on-site potential is shown in Fig. 30. It pushes the first particle of the chain along its
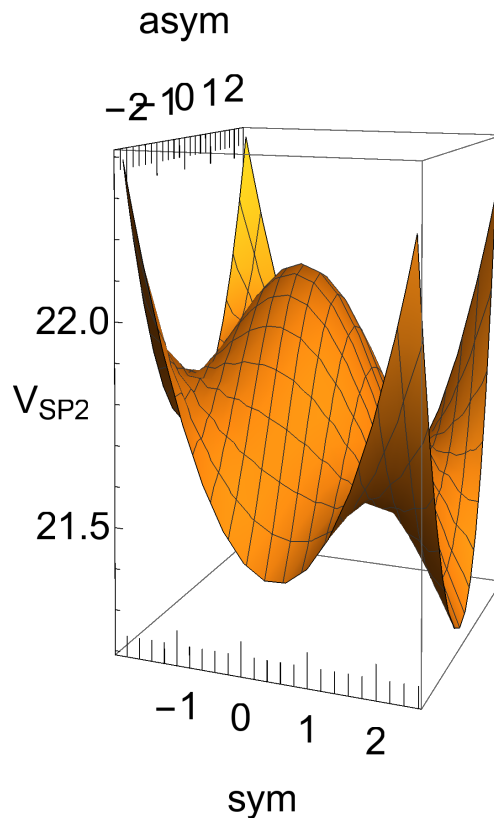
Fig. 28. 3D version of the 2D-schematic PES section of the 23-chain. The hill at the center is the central SP_2. One has to find the region around this SP_2 for a MEP of the chain through the mountains.

axis, and pulls the last particle into the same direction. All other particles are then moved by the springs between the particles. If one tilts the chain's site-potential with this force, one gets a change of the stationary points along the NT; and at the end, for a large enough force, a sliding of the chain will be enforced, see Fig. 31. That will be caused by a thermally activated transition between neighboring potential wells.

By the way, the two next still simpler directions, only push, or only pull [29] along the vectors $(1,0,...,0)^T$ or $(0,0,...,0,1)^T$ are not successful directions for an overall MEP of the chain. In the first case, the corresponding NT finds a way to the SP_1^{lb} and the intermediate minimum iMin2, however, then it goes wrong anywhere into the mountains of the PES. It does not cross the SP_1^{lt} and it also does not find to the 2π moved minimum. In the second case, the corresponding NT finds a way to the other valley of the SP_1^{rb} and the intermediate minimum iMin1, however, then it also goes wrong anywhere into the mountains. It does not cross the SP_1^{rt} and it also does not find to the 2π moved minimum. Both NTs also do not cross the SP_2 in the center of interest here. The two directions do not belong to the small channel for successful ways, compare the brown curves in Fig. 15.
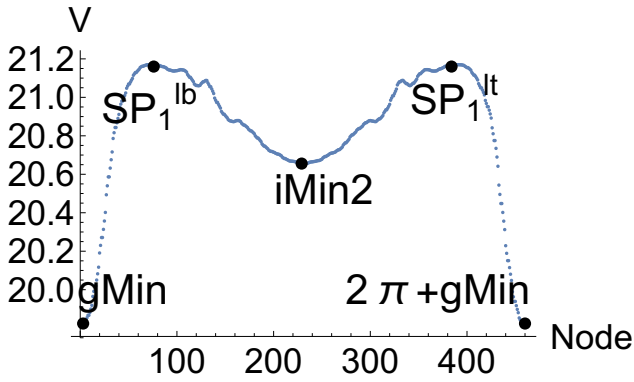
Fig. 29. Energy profile over the NT to the asymmetric direction $(1,0,...,0,1)^T$, compare Fig. 17. Start is the global minimum on the left hand side. The NT follows the valley uphill to the SP_1^{lb}, then turns to the intermediate minimum, iMin2, goes further uphill to SP_1^{lt}, and after crossing it, the NT goes downhill to the global minimum moved by 2π. All stationary points are marked by a black bullet.

Fig. 31. Tilting of the chain. Relative energy profiles over NTs to direction $(1,0,...,0,1)^T$. Start is the global minimum on the left hand side. The NT connects the SP_1^{lb}, the iMin2, the SP_1^{lt} and the global minimum moved by 2π. All curves are fixed at zero at the former final global minimum, for better comparison. From top to bottom we used the factors F=0.15, 0.1, 0.05, and 0.0. The red curve for F=0 corresponds to the profile in Fig. 29.

Fig. 30. Tilting of the chain at one of the global minimums, compare Fig. 3, right panel. The push and pull force, $\mathbf{f}$= 0.15 $(1,0,...,0,1)^T$, is used. The tilting force concerns the atoms x_1 and x_{23}. The atoms x_2 to x_{22} can then move by the spring forces in between.

7 Conclusion

Recently, experiments are done with laser-cooled and trapped ions for insights into friction processes [23,24,49,86–88]. The systems try to emulate the FK model (1) for a small number N, where the chain of the interesting particles slides under an external force over the fixed rigid sinusoidal potential. The FK model (1) is not realistic in every detail. But it is sufficiently complex for tests of basic concepts [89]. Thus any theoretical work to better understand such experiments is useful.

The PES (1) is given by an easy formula of the FK model. We can execute all calculations of NTs which determine the properties of the model. For comparison and confirmation we controlled the results of NT calculations by usual minimization procedures of the Mathematica program system because the PES of the FK model (1) is a usual surface where the known minimization procedures work. NTs are especially appropriate to the driven FK model by a tilting force. Of course, one can possibly find the existence of a low energy path through the PES without the theory of NTs. One has simply to do an opti-

mization for the global and intermediate minimums, and the SPs in between (if one is able to find these structures). However, an NT which follows more or less the low energy path gives the direction of the tilting which can move the chain through this path.

An interesting aspect of the example with N=23 particles is that usually not single particles form an anti-kink, a compression of a region of the chain. No, groups, like sets of triplets are involved in one step from a lower state to a higher one, and vice versa. Where two particles of the triplet stay in their well but the third particle moves over the top of the sinusoidal potential. Of course, this observation depends on the misfit parameter of 2/3 used here.

NTs allow us to drive them in very different directions over the PES. The standard direction $(1,...,1)^T$ is physically well understandable. It would cause a washboard potential. However, beginning with the case N=5 of the FK model [14], the standard direction is not a successful direction for a tilting with a low force. Our used directions deviate from the standard one. The corresponding valleys on the corrugated PES, which may also be very curvilinear, are better to follow by NTs which are adapted to the situation. So we work with a kind of tilting which concerns only parts of the chain with different weights. A possibly practicable case is the pure push and pull direction, $(1,0,...,0,1)^T$, see Fig.30. The push and pull force at the ends allows the different atoms to individually move by their spring forces, but not collectively by an equal force for all. If one atom surmounts its top of the site-up potential then another can relax and can transmit its energy to the former one. Such better directions of a tilting allow that individual valleys of the PES open, and so optimal forces can be gotten. Perhaps experimental workers can construct an experiment where such optimal forces are applied to the chain.

This paper treats the 'static' PES of the 23-dimensional FK-chain. Additionally we look for a 'step by step-series' of tilted 'static' effective PESs under an assumed external force. The amount of the force is even increased step by step. The tilting changes the barriers of the original PES. This is the information which we generate and discuss here. Which kind of dynamics the chain develops if it is really tilted, this is not discussed here. To study it would be a next step following the knowledge of the valley through the PES. But of course, the picture of changing barriers along a path for a movement may give already an impression what can happen.

This paper discusses a special chain with N=23 atoms for a special misfit parameter, 2/3. In a following paper we discuss different series of chains to different misfit parameters with the aim to test the possible length of the chain up to a 'critical' value where the theory above becomes questionable. We guess that the here found low energy paths through the PES continue to exist up to very high dimensions, in the kind 'global minimum $\rightarrow$ pre-SP $\rightarrow$ intermediate minimum $\rightarrow$ post-SP $\rightarrow$ global minimum moved by a_s'. However, it will be more and more difficult to find a corresponding search direction for a unique NT which follows the path.

Disclosure statement

No potential conflict of interest was reported by the authors.

Authors contributions

All the authors were involved in the preparation of the manuscript. All the authors read and approved the final manuscript.

Funding

Supplemental Material

The authors confirm that the data supporting the findings of this study are available within the article and its Supplemental Material (SM).

References

1. O.M. Braun, Y.S. Kivshar, Phys. Rep. **306**, 1 (1998)
2. J. Tekić, P. Mali, *The ac driven Frenkel-Kontorova model* (University of Novi Sad, Novi Sad, 2015)
3. O. Braun, T. Dauxois, M. Paliy, M. Peyrard, B. Hu, Physica D **123**, 357 (1998)
4. S. Brazovskii, T. Nattermann, Adv. Phys. **53**, 177 (2004)
5. M. Johansson, G. Kopidakis, S. Lepri, S. Aubry, Europhys. Lett. **86**, 10009 (2009)
6. R. Khomeriki, Eur. Phys. J. B **72**, 257 (2009)
7. S. Watanabe, H.S.J. van der Zant, S.H. Strogatz, T.P. Orlando, Physica D **97**, 429 (1996)
8. O. Braun, A. Naumovets, Surf. Sci. Rep. **60**, 79 (2006)
9. S. Flach, A.V. Gorbach, Phys. Rep. **467**, 1 (2008)
10. N. Manini, O.M. Braun, E. Tosatti, R. Guerra, A. Vanossi, J. Phys. **28**, 134006 (2016)
11. A. Vanossi, N. Manini, M. Urbakh, S. Zapperi, Rev. Mod. Phys **85**, 529 (2013)
12. N.I. Gershenzon, G. Bambakidis, E. Hauser, A. Ghosh, K.C. Creager, Geophys. Res. Lett. **38**, L01309 (2011)
13. T. Zanca, F. Pellegrini, G.E. Santoro, E. Tosatti, PNAS p. online (2018)
14. W. Quapp, J.M. Bofill, Mol. Phys. (2019) doi.org/10.1080/00268976.2019.1576930
15. W. Quapp, J. Theoret. Comput. Chem. **2**, 385 (2003)
16. S.R. Sharma, B. Bergersen, B. Joos, Phys. Rev. B **29**, 6335 (1984)
17. Y. Braiman, J. Baumgarten, J. Jortner, J. Klafter, Phys. Rev. Lett. **65**, 2398 (1990)
18. S.L. Shumway, J.P. Sethna, Phys. Rev. Lett. **67**, 995 (1991)
19. C. Baesens, R.S. MacKay, Nonlinearity **11**, 949 (1998)
20. T. Strunz, F.J. Elmer, Phys. Rev. E **58**, 1601 (1998)
21. N. Theodorakopoulos, M. Peyrard, R.S. MacKay, Phys. Rev. Lett. **93**, 258101 (2004)
22. I.D. Mikheikin, M.Y. Kuznetsov, E.V. Makhonina, V.S. Pervov, J. Mater. Synth. Process. **10**, 53 (2002)
23. A. Bylinskii, D. Gangloff, I. Counts, V. Vuletić, Nature Materials **15**, 717 (2016)
24. J. Kiethe, R. Nigmatullin, D. Kalincev, T. Schmirander, T.E. Mehlstäubler, Nature Commun. **8**, 15364 (2017)
25. S.N. Coppersmith, Phys. Rev. A **36**, 3375 (1987)
26. B. Hu, J.Y. Zhu, Phys. Rev. E **65**, 016202 (2001)
27. A. Patrykiejew, S. Sokolowski, Cond. Mat. Phys. **17**, 43601:1 (2014)
28. J. Zhang, X. Chen, R. Chen, L. Nie, Z. Zheng, Eur. Phys. J. B **87**, 122 (2014)
29. X. Zhang, L. Nie, K. Ma, J. Zhang, J. Wu, F. Ye, C. Xiao, Modern Phys. Lett. B **32**, 1850017 (2018)
30. P. Bak, Rep. Prog. Phys. **45**, 587 (1982)
31. J.M. Bofill, J. Ribas-Ariño, S.P. García, W. Quapp, J.Chem.Phys. **147**, 152710 (2017)
32. W. Quapp, B. Schmidt, Theor. Chem. Acc. **128**, 47 (2011)
33. B. Schmidt, W. Quapp, Theor. Chem. Acc. **132**, 1305 (2012)
34. C. Baesens, R.S. MacKay, Nonlinearity **17**, 567 (2004)
35. Z. Zheng, B. Hu, G. Hu, Physical Review B **58**, 5453 (1998)
36. O.M. Braun, A.R. Bishop, J. Röder, Phys. Rev. Let. **79**, 3692 (1997)
37. O.M. Braun, B. Hu, A. Zeltser, Phys. Rev. E **62**, 4235 (2000)
38. O.M. Braun, H. Zhang, B. Hu, J. Tekić, Phys. Rev. E **67**, 06602 (2003)

39. A.B. Kolton, D. Dominguez, N. Gronbech-Jensen, Phys. Rev. Lett. **86**, 4112 (2001)
40. S. Slijepčević, Chaos **25**, 083108 (2015)
41. I. Sokolović, P. Mali, J. Odavić, S. Radosevic, S.Y. Medvedeva, A.E. Botha, Y.M. Shukrinov, J. Tekić, Phys. Rev. E **96**, 022210 (2017)
42. J. Odavić, P. Malik, J. Tekić, M. Pantic, M. Pavkov-Hrvojevic, Commun. Nonlinear Sci. Numer. Simulat. **47**, 100 (2017)
43. H. Li, S. Liu, Discr. Dyn. Nat. Soc. **47**, 7081804 (2018)
44. M. Hirano, K. Shinjo, Phys. Rev. B **41**, 11837 (1990)
45. A. Socoliuc, R. Bennewitz, E. Gnecco, E. Meyer, Phys. Rev. Lett. **92**, 134301 (2004)
46. M. Dienwiebel, G.S. Verhoeven, N. Pradeep, J.W.M. Frenken, J.A. Heimberg, H.W. Zandbergen, Phys. Rev. Lett. **92**, 126101 (2004)
47. E. Gnecco, S. Maier, E. Meyer, J. Phys.: Cond. Mat. **20**, 354004 (2008)
48. E. Meyer, E. Gnecco, Friction **2**, 106 (2014)
49. A. Bylinskii, D. Gangloff, V. Vuletić, Sci. **348**, 1115 (2015)
50. W. Quapp, M. Hirsch, O. Imig, D. Heidrich, J. Comput. Chem. **19**, 1087 (1998)
51. W. Quapp, M. Hirsch, D. Heidrich, Theor. Chem. Acc. **100**, 285 (1998)
52. J.M. Bofill, J.M. Anglada, Theor. Chem. Acc. **105**, 463 (2001)
53. R. Crehuet, J.M. Bofill, J.M. Anglada, Theor. Chem. Acc. **107**, 130 (2002)
54. W. Quapp, J. Theoret. Comput. Chem. **2**, 385 (2003)
55. W. Quapp, J.M. Bofill, Theoret. Chem. Acc. **135**, 113 (2016)
56. W. Quapp, J.M. Bofill, J. Ribas-Ariño, J.Phys.Chem.A **121**, 2820 (2017)
57. M. Hirsch, W. Quapp, J. Molec. Struct., THEOCHEM **683**, 1 (2004)
58. B. Peters, A. Heyden, A.T. Bell, A. Chakraborty, J.Chem.Phys. **120**, 7877 (2004)
59. W. Quapp, J.Chem.Phys. **122**, 174106 (2005)
60. D.E. Makarov, J. Chem. Phys. **144**, 030901 (2016)
61. W. Quapp, J.M. Bofill, J. Comput. Chem. **37**, 2467 (2016)
62. M. Basilevsky, A. Shamov, Chemical Physics **60**, 347 (1981)
63. D.K. Hoffmann, R.S. Nord, K. Ruedenberg, Theor. Chim. Acta **69**, 265 (1986)
64. W. Quapp, Theoret. Chim. Acta **75**, 447 (1989)
65. H.B. Schlegel, Theor. Chim. Acta **83**, 15 (1992)
66. J.Q. Sun, K. Ruedenberg, J. Chem. Phys. **98**, 9707 (1993)
67. M. Hirsch, W. Quapp, Chem. Phys. Lett. **395**, 150 (2004)
68. J.M. Bofill, W. Quapp, M. Caballero, J. Chem. Theory Comput. **8**, 927 (2012)
69. I. Garcia-Mata, O.V. Zhirov, D.L. Shepelyansky, Eur. Phys. J. D **41**, 325 (2007)
70. D. Heidrich, W. Quapp, Theor. Chim. Acta **70**, 89 (1986)
71. Y.G. Khait, A.I. Panin, A.S. Averyanov, Int. J. Quant. Chem. **54**, 329 (1994)
72. P. Chaudhury, S. Bhattacharyya, Chemical Physics **241**, 313 (1999)
73. R.M. Minyaev, I.V. Getmanskii, W. Quapp, Russ. J. Phys. Chem. **78**, 1494 (2004)
74. G.S. Ezra, S. Wiggins, J. Phys. A **42**, 205101 (2009)
75. P. Collins, G.S. Ezra, S. Wiggins, J. Chem. Phys **134**, 244105 (2011)
76. J.M. Bofill, W. Quapp, M. Caballero, Chem. Phys. Lett. **583**, 203 (2013)
77. W. Quapp, J.M. Bofill, Int. J. Quantum Chem. **115**, 1635 (2015)
78. W. Quapp, E. Kraka, D.Cremer, J. Phys. Chem. **111**, 11287 (2007)
79. H. Joo, E. Kraka, W. Quapp, D.Cremer, Molec. Phys. **105**, 2697 (2007)
80. M. Hirsch, W. Quapp, D. Heidrich, Phys. Chem. Chem. Phys. **1**, 5291 (1999)
81. W. Quapp, V. Melnikov, Phys. Chem. Chem. Phys. **3**, 2735 (2001)
82. W. Quapp, J. Bofill, A. Aguilar-Mogas, Theor. Chem. Acc. **129**, 803 (2011)
83. W. Quapp, J. Math. Chem. **54**, 137 (2015)
84. D.R. Yarkony, J. Chem. Phys. **123**, 204101 (2005)
85. W. Quapp, J.M. Bofill, M. Caballero, Chem. Phys. Lett. **541**, 122 (2012)
86. T. Pruttivarasin, M. Ramm, I. Talukdar, A. Kreuter, H. Haeffner, New J. Phys. **13**, 075012 (2011)
87. E. Panizon, G.E. Santoro, E. Tosatti, G. Riva, N. Manini, Phys. Rev. B **97**, 104104 (2018)
88. D. Mandelli, R. Guerra, W. Ouyang, M. Urbakh, A. Vanossi, Phys. Rev. Materials **2**, 046001 (2018)
89. M. Weiss, F.J. Elmer, Z. Physik B Cond. Matter **69**, 55 (1997)

A Model for a Driven Frenkel-Kontorova Chain

W. Quapp,[a] and J. M. Bofill[b]

[a]Mathematisches Institut, Universität Leipzig,
PF 100920, D-04009 Leipzig, Germany
Email: quapp@uni-leipzig.de
[b]Departament de Química Inorgànica i Orgànica,
Secció de Química Orgànica, and
Institut de Química Teòrica i Computacional,
(IQTCUB), Universitat de Barcelona,
Martí i Franquès 1, 08028 Barcelona, Spain
Email: jmbofill@ub.edu

Supplemental Material

xxxxxxxxxxxxxxx SM xxxxxxxxxxxxxxxx

1 Data of the discussed structures of the 23-particle chain

1.1 a) The 'left' minimum is at energy 19.824175.

The structure is shown in the text.
Coordinates

```
 0.3010   4.78629   8.2743 12.6753 17.1849
20.699   25.1744  29.6916 33.2206 37.7223
42.2472  45.7856  50.297  54.84   58.3925
62.908   67.4994  71.0919 75.6031 80.3176
84.0536  88.4852  93.4143
```

The 5 lowest eigenvalues are:
0.3565, 0.2293, 0.1675, 0.1132, 0.0000402.
The lowest eigenvector is

```
0.0309, 0.0600, 0.0987, 0.0851, 0.1543,
0.2454, 0.1913, 0.3163, 0.5759, 0.3015,
0.2499, 0.4041, 0.2325, 0.128,  0.1472,
0.0977, 0.0505, 0.0533, 0.0368, 0.0193,
0.0207, 0.0131, 0.0067
```

1.1 b) The 'right' minimum is

Coordinates

```
 0.8314,  5.7595, 10.188,  13.9256, 18.6413,
23.1508, 26.744,  31.3368, 35.8509, 39.4036,
43.9479, 48.4581, 51.9966, 56.5227, 61.0232,
64.5523, 69.0706, 73.5450, 77.0593, 81.5701,
85.9700, 89.4589, 93.9452
```

Its structure is shown in the text.

2 Global region around the central high SP of index 2

2.1 The SP$_2$

There is the central region around an SP$_2$ at an energy 22.099. The structure is shown in the text.
Coordinates

```
 3.3442   7.33177  12.186   16.6691  20.3323
24.9916  29.5103  33.0845  37.654   42.1783
45.7296  50.2655  54.8013  58.3527  62.877
67.4464  71.0207  75.5393  80.1987  83.8619
88.3449  93.1992  97.1868
```

The 6 lowest eigenvalues are:
0.3768, 0.2581, 0.1717, 0.1247, -0.3813, -0.3813.

Two negative degenerated eigenvectors are

```
0.6445 0.2589 0.1012 0.0759 0.0361
0.0133 0.0087 0.0045 0.0017 0.0011
0.0007 0.0004 0.0007 0.0011 0.0017
0.0045 0.0087 0.0133 0.0361 0.0759
0.1012 0.2589 0.6445
1.ev  antisymmetric
```

```
-0.6445 -0.2589 -0.1012 -0.0759 -0.0361
-0.0133 -0.0087 -0.0045 -0.0016 -0.001
-0.0004  0.0     0.0004  0.001   0.0016
 0.0045  0.0087  0.0133  0.0361  0.0759
 0.1012  0.2589  0.6445
 2. ev    symmetric
```

We show a Figure with NTs connecting the central SP$_2$ with other stationary points.
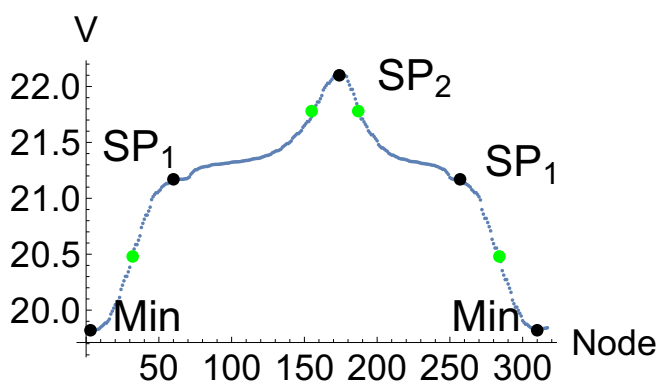
Fig. 1. Energy profile over a path formed by NTs from the 'left' minimum of Fig. 3 of the text to the 2π displaced 'left' minimum. The global barrier is 2.275 units. The green bullets are the main BBPs. The SP$_2$ is depicted in Fig. 4 in the text. The SP$_1$ are the 'left' ones, SP_1^{lb} and SP_1^{lt}.

2.2 The SP$_1$ of the circle around the central SP$_2$

SP$_1^{rb}$ at 21.2106

```
0.86463    5.81427   10.312    14.0344   18.7515
23.3708   27.0083   31.5997   36.3738   40.1779
44.5974   49.5938   53.9679   57.8101   62.6049
67.1746   70.8119   75.4412   80.1136   83.7859
88.3192   93.1997   97.2137
```

EW:
0.26125, 0.1875, 0.12561, 0.02687, -0.38473

```
minus EV:
0.0       0.0       0.0       0.0       0.0
0.00001   0.00002   0.00002   0.00006   0.00015
0.00017   0.00039   0.00107   0.00126   0.00231
0.00651   0.01086   0.01802   0.05010   0.10162
0.14053   0.36529   0.91295
```

A force, **f**, in this direction would push mainly the right part of the chain, with increasing components.

SP$_1^{rt}$

```
3.31726    7.33126   12.2118   16.7451   20.4174
25.0898   29.7191   33.3564   37.9261   42.7209
46.5631   50.9372   55.9336   60.3531   64.1572
68.9313   73.5227   77.1602   81.7795   86.4966
90.219    94.7167   99.6663
```

EW:
0.26125, 0.1875, 0.12561, 0.02687, -0.38473

```
minus EV:
0.91295   0.36529   0.14053   0.10162   0.0501
0.01802   0.01086   0.00651   0.00231   0.00126
0.00107   0.00039   0.00017   0.00015   0.00006
0.00002   0.00002   0.00001   0.0       0.0
0.0       0.0       0.0
```

A force, **f**, in this direction would push mainly the left part of the chain, with increasing components to the left hand side.

SP$_1^{lb}$ at 21.16990

```
3.90152    7.40144   11.8007   15.5069   19.4129
23.8527   27.3346   31.6239   36.1196   39.6154
44.0521   48.5584   52.0741   56.5616   61.062
64.5822   69.0863   73.5616   77.0721   81.5773
85.9785   89.4647   93.9484
```

EW:
0.30922, 0.20752, 0.13871, 0.08378, -0.20945

```
minus EV:
0.8263    0.40039   0.23342   0.28363   0.11532
0.06867   0.05609   0.02216   0.01456   0.00989
0.00394   0.00274   0.00174   0.0007    0.0005
0.00031   0.00012   0.00009   0.00005   0.00002
0.00002   0.0       0.0
```

SP$_1^{lt}$

```
6.57531   11.0573   14.5433   18.9488   23.4539
26.9652   31.4425   35.9465   39.4671   43.9682
48.4553   51.971    56.4775   60.9130   64.4084
68.9039   73.1896   76.6719   81.1102   85.0077
88.7209   93.1195   96.6123
```

EW:
0.30922, 0.20752, 0.13871, 0.08378, -0.20945

```
minus EV:
0.0       0.0       0.00002   0.00002   0.00005
0.00001   0.00012   0.00031   0.0005    0.0007
0.00174   0.00274   0.00394   0.00989   0.01456
0.02216   0.05609   0.06867   0.11532   0.28363
0.23342   0.40039   0.8263
```

3 Intermediates

3.1 iMin1

The intermediate minimum is shown in the text. It is at the level 20.437.
Coordinates

```
0.9172,   5.8999, 10.5087, 14.2336, 18.9539,
23.7785, 27.6263, 32.0778, 37.1438, 41.6827,
45.4756, 50.2655, 55.0554, 58.8483, 63.3871,
68.4532, 72.9047, 76.7525, 81.577,  86.2973,
90.0223, 94.6311, 99.6138
```

Lowest eigenvalues are 0.3151, 0.2505, 0.1697, 0.0721, 0.0366.

3.2 iMin2

The intermediate minimum is shown in the text. The energy is 20.6556.
Coordinates

```
6.472,   10.8485, 14.2358, 18.6182, 22.7713,
26.221,  30.5566, 34.1347, 38.1232, 42.5231,
45.9293, 50.2655, 54.6017, 58.0079, 62.4078,
66.3962, 69.9744, 74.3099, 77.7597, 81.9128,
86.2952, 89.6825, 94.059
```

Lowest eigenvalues are 0.3712, 0.2357, 0.1866, 0.0404, 0.0149.

3.3 VRIs in the iMin1 bowl

The VRI1 is at energy 20.6710 with $|Ag|$=1.459E-002

```
1.3712    6.1583   10.7924   14.6490   19.1809
23.9519   27.8818   32.2208   37.2137   41.7468
45.5090   50.2653   55.0214   58.7835   63.3170
68.3101   72.6493   76.5791   81.3501   85.8819
89.7386   94.3727   99.1596
```

```
        vridir (grad)
```

```
 0.38186  0.02845  -0.20198  0.19658  0.08618
-0.08386 -0.02657   0.06689 -0.00682 -0.01621
 0.00494  0.00002  -0.00506  0.01610  0.00684
-0.06695  0.02677   0.08376 -0.08617 -0.19669
 0.20205 -0.02832  -0.38199
```

VRI2 at energy 20.9200 with $|Ag|$=3.843E-003.

```
 1.6079    6.2715  10.8747  14.7628  19.2271
23.9350   27.8133  32.1958  37.1972  41.7251
45.4988   50.2652  55.0313  58.8048  63.3333
68.3348   72.7173  76.5957  81.3038  85.7682
89.6563   94.2595  98.9231
```

```
        vridir (grad)
```

```
 0.52379  0.04876  -0.27730  0.23422  0.12480
-0.10143 -0.05922   0.08427 -0.00770 -0.01931
 0.00589  0.00004  -0.00602  0.01918  0.00773
-0.08427  0.05939   0.10124 -0.12474 -0.23413
 0.27724 -0.04864  -0.52383
```

The VRI3 is at energy 21.0872 with $|Ag|$= 1.507E-003

```
 1.7387    6.3281   10.8995   14.7944   19.2368
23.9082   27.7564   32.1745   37.1823   41.7048
45.4894   50.2652   55.0406   58.8248   63.3480
68.3561   72.7741   76.6223   81.2940   85.7365
89.6315   94.203    98.7925
```

```
        vridir (grad)
```

```
 0.58677   0.06379  -0.32116   0.24454  0.14988
-0.1184   -0.07490   0.09879  -0.00886 -0.02270
 0.00672   0.00005  -0.00683   0.02249  0.00888
-0.0987    0.07509   0.11808  -0.14977 -0.2445
 0.32114  -0.06366  -0.586716
```